Available online at www.sciencedirect.com
SCIENCE DIRECT®
PERGAMON
International Journal of Heat and Mass Transfer 46 (2003) 2645–2653
International Journal of HEAT and MASS TRANSFER
www.elsevier.com/locate/ijhmt

Simultaneous reconstruction of temperature distribution, absorptivity of wall surface and absorption coefficient of medium in a 2-D furnace system

Huai-Chun Zhou *, Shu-Dong Han

State Key Laboratory of Coal Combustion, Huazhong University of Science and Technology, Wuhan 430074, PR China

Received 23 November 2001; received in revised form 29 November 2002

Abstract

For a 2-D furnace system filled with a gray medium, surrounded by gray emitting/absorpting and diffusely reflecting wall surfaces, the temperature distribution is reconstructed using an improved Tikhonov regularization method with radiative energy images detected from the boundary of the furnace, uniform absorptivity of both the wall surfaces and the medium being updated from the temperature images grasped from the boundary too. These steps are taken alternately till a convergence is reached. The measurement errors with normal distribution of standard square deviation of 0.01 are taken into consideration for the radiative energy image and temperature image data. The reconstruction errors for radiative properties vary from 1.45% to 10.75%, and for the highest temperature are within 2%. Comparatively, the reconstruction result for the sharper temperature distribution is not as good as that for the smoother temperature distribution. The applicability of the proposed method may be practically valuable.

Keywords: 2-D temperature distribution; Image processing; Radiative properties

1. Introduction

Radiation is the predominant mode of heat transfer in large-scale, particle-laden combustion systems, such as pulverized-coal fired furnaces [1]. Efficient monitoring methods for industrial combustion processes can come from the solutions of inverse radiative transfer problems in the furnaces. The temperature distributions in 2-D systems were estimated from the measurement of the outgoing radiation intensities when the optical properties of the medium were known [2]. The optical thickness, the single scattering albedo and the phase function were estimated simultaneously by inverse analysis, from the knowledge of radiation intensity taken at the boundary surfaces of a plane-parallel medium [3]. Mostly, the radiative intensities measured from the boundary of a system were used as the only input data for the solution of the inverse radiative problems [1–4]. However, temperature profile/image data measured from the system boundary can be used as a kind of additional input data, and the temperature distribution and scattering albedo profile in a 1-D system were reconstructed simultaneously from the radiative energy and temperature profiles measured from the boundaries [5]. 2-D temperature distribution in a rectangular enclosure has been reconstructed from radiative energy images detected from the corners of the system [6]. But the simultaneous reconstruction of the temperature distribution and the radiative properties has not been studied more often.

A non-iterative method for the reconstruction of temperature distribution will be helpful to reconstruct simultaneously the temperature distribution and radiative properties. Tikhonov [7] first proposed a regularization method in 1963, and recent researches in this field seem very active [8–10]. Reginska [9] put forward a method to determine the regularization parameter, and Holloway et al. [10] modified this method through giving

* Corresponding author. Tel./fax: +86-27-8754-5526.
E-mail address: hczhou@mail.hust.edu.cn (H.-C. Zhou).

0017-9310/03/$ - see front matter
doi:10.1016/S0017-9310(03)00017-6

Nomenclature

A, $\mathbf{A}$	constants and their matrix defined in Eq. (2)
C_1, C_2	Planck's constants
$\mathbf{D}$	regularization operator
E, $\mathbf{E}$	radiative energy (W) and its vector (W)
m	number of surface elements
n	number of medium elements
Rd	READ value referring to the ratio of radiative energy received by image pixels
R_T	reconstruction error for temperature expressed in Eq. (16)
S	area of surface elements (m^2)
T, $\mathbf{T}$	temperature in the system (K) and vector of its fourth power (K^4)
T_C, $\mathbf{T}_C$	temperature (K) and its matrix (K^4) measured by Eq. (3)
T_M, $\mathbf{T}_M$	temperature (K) and its matrix (K^4) measured by Eq. (4)
V	volume of medium elements (m^3)
α	regularization parameter
δ	refers to small increment
k_a	absorption coefficient of medium (1/m)
λ_1, λ_2	two representative wavelengths used in Eq. (3) (nm)
σ	Boltzmann constant standard square deviation
ε	absorptivity of surface (/)
ς	random variable
Δ	refers to updating value

Superscripts

r	iteration number
T	transposed matrix

Subscripts

meas	measured
min	minimum
recons	reconstructed

a finite difference regularizer and successfully obtained the reconstruction of 1-D spatially resolved plasma optical emission.

In this paper, temperature image data together with radiative energy image data will be used to reconstruct 2-D temperature distribution, absorptivity of wall surface and absorption coefficient of medium in a 2-D furnace system filled with gray emitting/absorption medium and surrounded by gray emitting/absorption and diffusely reflecting wall surface. The temperature distributions will be reconstructed from the radiative energy images using an improved Tikhonov regularization method. The two radiative properties are then updated from the temperature images. These two steps are taken alternately till a convergence is reached.

2. Method proposed

2.1. Basic consideration

Consider a 2-D rectangular furnace filled with a gray emitting/absorption medium and surrounded by gray emitting/absorption and diffusely reflecting surfaces [6,11]. The absorption coefficient of the medium, k_a (m^{-1}), is assumed be uniform, and the absorptivity of the surfaces, ε (/), is also uniform. The temperature distribution of the system is T_i, $i = 1, \ldots, m+n$, where m is the elements divided for the surface, and n is the zones divided for the medium. CCD cameras are mounted in the corners of the system with larger viewing angles than the cross angles of the corners. The total radiative energy received by the jth image pixel in one CCD camera can be expressed as we reported in [6]

$$E(j) = \sum_{i=1}^{m} \mathrm{Rd}(i \to j)\varepsilon\sigma T_i^4 \Delta S_i + \sum_{i=m+1}^{m+n} \mathrm{Rd}(i \to j) 4k_a \sigma T_i^4 \Delta V_i, \quad (1)$$

which is transferred into a matrix equation as

$$\mathbf{E} = \mathbf{AT}, \quad (2)$$

where

$$A(i,j) = \begin{cases} \mathrm{Rd}(i \to j)\varepsilon\sigma\Delta S_i, & \text{when } i \leqslant m, \\ \mathrm{Rd}(i \to j) 4k_a\sigma\Delta V_i, & \text{when } i > m, \end{cases}$$

$$T(i) = T_i^4.$$

In these equations, $4k_a\sigma T_i^4 \Delta V_i$ refers to the total energy emitted by the ith medium element with absorption coefficient k_a, temperature T_i and volume ΔV_i, σ is the Boltzmann constant, and $\varepsilon\sigma T_i^4 \Delta S_i$ refers to the total energy emitted by the ith surface element with emissivity ε, temperature T_i and area ΔS_i. $\mathrm{Rd}(i \to j)$, also called READ values [6,11], refer to the ratio of energy received by the jth image pixel element to the total energy emitted by the ith system element. The calculation method for $\mathrm{Rd}(i \to j)$ and the radiative energy images $\mathbf{E}$ has been described for 2-D cases [12], and will not be given here.

Besides the radiative energy images used as input data, the temperature images are also measured as input data in this paper. A monochromatic radiative temperature image monitoring method was given in [13]. In this

method, a reference temperature in a certain direction j_0 within the viewing field of the image-formation process is measured through using the two-color method. The measuring direction of the reference temperature is suggested close the highest temperature zone inside the system. Selecting two representative wavelengths, λ_1, λ_2, substituting the total radiative energy, σT_i^4, in Eq. (1) with the monochromatic energy $(C_1/\lambda^5)\exp(-C_2/\lambda T_i)$, repeating the forward calculation (due to the gray characteristics of the medium, the whole and monochromatic radiative properties are the same, then the values of Rd do not need to be calculated again), two monochromatic radiative images $E_{\lambda_1}(j)$, $E_{\lambda_2}(j)$ can be obtained. Through using the two-color method (see, for example, [14]), a kind of temperature $T_C(j)$ can be calculated from $E_{\lambda_1}(j)/E_{\lambda_2}(j)$, that is,

$$T_C(j) = -C_2\left(\frac{1}{\lambda_1}-\frac{1}{\lambda_2}\right)\Bigg/\ln\left[\frac{E_{\lambda_1}(j)}{E_{\lambda_2}(j)}\frac{\lambda_1^5}{\lambda_2^5}\right]. \tag{3}$$

But an other kind of temperature image $T_M(j)$ is chosen as the boundary temperature image in this study. In order to calculate $T_M(j)$, one temperature in pixel j_0 from $\mathbf{T}_C$, that is $T_C(j_0)$, is taken as a reference temperature. Then, $T_M(j)$ can be deduced from one monochromatic radiative image $E_{\lambda_1}(j)$ (or $E_{\lambda_2}(j)$) with the aid of the reference temperature as [13]

$$T_M(j) = 1\Bigg/\left(\frac{1}{T_C(j_0)}-\frac{\lambda_1}{C_2}\ln\left(\frac{E_{\lambda_1}(j)}{E_{\lambda_1}(j_0)}\right)\right). \tag{4}$$

Obviously, radiative temperature image $\mathbf{T}_M$ is a function of the temperature distribution $\mathbf{T}$, radiative properties k_a and ε, that is, $\mathbf{T}_M = f(k_a, \varepsilon, \mathbf{T})$. As discussed from the reconstruction results below, obvious difference may exist between the two kinds of temperature images, $\mathbf{T}_C$ and $\mathbf{T}_M$, we select $\mathbf{T}_M$ for the simultaneous reconstruction. Thus, for a given gray emitting/absorption, 2-D rectangular furnace system, its temperature distribution $\mathbf{T}$ (including surface temperature and medium temperature), the absorptivity ε of the diffusely reflecting surface and the absorption coefficient k_a, the radiative energy images $\mathbf{E}$ in its several corners and the radiative temperature images $\mathbf{T}_M$ in the same corners can be obtained from Eqs. (1)–(4).

The inverse problem is then described as below. Given the radiative energy images $\mathbf{E}$ and the radiative temperature images $\mathbf{T}_M$ as input data, added by random errors with zero average value and normal distribution of standard square deviation σ, that is

$$\begin{cases}\mathbf{E}_{meas} = \mathbf{E}(1+\sigma\varsigma),\\ \mathbf{T}_{M,meas} = \mathbf{T}_M(1+\sigma\varsigma),\end{cases} \tag{5}$$

where the range of random variables ς is chosen as $-2.576 < \varsigma < 2.576$, which represents the 99% confidence bound for the measured data. Then, the temperature distribution $\mathbf{T}$ of the system and the radiative properties ε and k_a are to be reconstructed from $\mathbf{E}_{meas}$ and $\mathbf{T}_{M,meas}$.

2.2. Reconstruction of 2-D temperature distribution by regularization method

To reconstruct the temperature distribution, $\mathbf{T}_{recons}$, determined by

$$\mathbf{E}_{meas} = \mathbf{A}\mathbf{T}_{recons} \tag{6}$$

a modified Tikhonov regularization method was proposed in [10], of which the basic principle is to find a $\mathbf{T}$ that minimizes

$$R(\mathbf{T},\alpha) = \|\mathbf{E}_{meas} - \mathbf{A}\mathbf{T}\|^2 + \alpha\|\mathbf{D}\mathbf{T}\|^2, \tag{7}$$

where $\mathbf{D}$ is a regularization operator such that $\mathbf{DT}$ is expected to be effective for a reconstructed parameter which is continuously distributed in space. The regularization parameter α also plays an important role in reconstruction, as suggested in [10]:

$$\alpha(\mathbf{E}_{meas}) \approx 2\|\mathbf{E}_{meas} - \mathbf{A}\mathbf{T}(0)\|^2/\|\mathbf{D}\mathbf{T}(0)\|^2, \tag{8}$$

where $\mathbf{T}(0)$ is the least-square solution of Eq. (6), and the solution of Eq. (6) under the minimization of Eq. (7) is derived in [10] as

$$\mathbf{T}'_{recons} = (\mathbf{A}^T\mathbf{A} + \alpha\mathbf{D}^T\mathbf{D})^{-1}\mathbf{A}^T\mathbf{E}_{meas}. \tag{9}$$

However, for the reconstruction of 2-D temperature distribution in furnaces, the modified Tikhonov regularization method needs to be improved in selecting the regularization operator $\mathbf{D}$. As shown in Fig. 1, there are three kinds of elements which have different relationships with other adjacent elements: (a) the elements in the crank points; (b) the elements along the edges except those in (a); and (c) all the rest elements inside the faces elements. For these three kinds of elements, the corresponding elements in the matrix $\mathbf{DT}$ are selected as

$$\text{Elements in } DT \text{ corresponding to } T_0 = \begin{cases} T_0 - (1/2)(T_1+T_2) & \text{for } T_0 \text{ belong to (a)},\\ T_0 - (1/3)(T_1+T_2+T_3) & \text{for } T_0 \text{ belong to (b)},\\ T_0 - (1/4)(T_1+T_2+T_3+T_4) & \text{for } T_0 \text{ belong to (c)}.\end{cases} \tag{10}$$

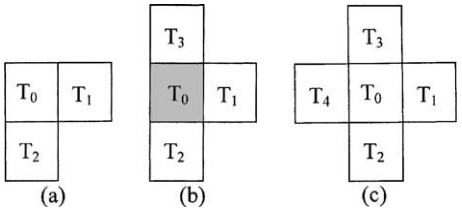

Fig. 1. Three spatial relationships for elements in a 2-D rectangular space.

The regularization operator **D** has two features: all the diagonal elements are 1.0, and the sum of the elements in every row is 0.

Actually, the fourth power of the temperature in a furnaces should be higher than a positive limitation, $T_{\min}$ (for instance, it is selected as 200^4 in this paper). A post treatment is adopted in this paper. After $\mathbf{T}'_{\text{recons}}$ is obtained through using the regularization method, a new solution, $\mathbf{T}_{\text{recons}}$, is defined as

$$T_{\text{recons},i} = \begin{cases} T'_{\text{recons},i} & \text{if } T'_{\text{recons},i} > T_{\min}, \\ T_{\min} & \text{if } T'_{\text{recons},i} \leqslant T_{\min}. \end{cases} \tag{11}$$

Obviously, $\mathbf{T}_{\text{recons}}$ is a quasi-optimal solution of Eq. (7). This revised Tikhonov regularization method has been successfully used in reconstruction of three-dimensional temperature distributions in a large-scale furnace [15].

2.3. Updating the radiative properties

The temperature distribution is $\mathbf{T}^{(r)}$ after rth iteration, and the radiative properties are $k_a^{(r)}$ and $\varepsilon^{(r)}$, respectively. We need to calculate the updating values $\Delta k_a^{(r)}$ and $\Delta\varepsilon^{(r)}$ from the radiative temperature images $\mathbf{T}_{\text{M,meas}}$. With the first approximation

$$\mathbf{T}_{\text{M,meas}} \approx \mathbf{T}_{\text{M}}^{(r)} + \left(\frac{\partial \mathbf{T}_{\text{M}}^{(r)}}{\partial k_a} \; \frac{\partial \mathbf{T}_{\text{M}}^{(r)}}{\partial \varepsilon} \right) \begin{pmatrix} \Delta k_a^{(r)} \\ \Delta \varepsilon^{(r)} \end{pmatrix}, \tag{12}$$

under the least-square meaning, we have

$$\begin{pmatrix} \Delta k_a^{(r)} \\ \Delta \varepsilon^{(r)} \end{pmatrix} = \left(\left(\frac{\partial \mathbf{T}_{\text{M}}^{(r)}}{\partial k_a} \; \frac{\partial \mathbf{T}_{\text{M}}^{(r)}}{\partial \varepsilon} \right)^{\text{T}} \left(\frac{\partial \mathbf{T}_{\text{M}}^{(r)}}{\partial k_a} \; \frac{\partial \mathbf{T}_{\text{M}}^{(r)}}{\partial \varepsilon} \right) \right)^{-1} \times \left(\frac{\partial \mathbf{T}_{\text{M}}^{(r)}}{\partial k_a} \; \frac{\partial \mathbf{T}_{\text{M}}^{(r)}}{\partial \varepsilon} \right)^{\text{T}} (\mathbf{T}_{\text{M,meas}} - \mathbf{T}_{\text{M}}^{(r)}), \tag{13}$$

where $\mathbf{T}_{\text{M}}^{(r)} = f(k_a^{(r)}, \varepsilon^{(r)}, \mathbf{T}^{(r)})$. In order to calculate $\partial \mathbf{T}_{\text{M}}^{(r)}/\partial k_a$, $\partial \mathbf{T}_{\text{M}}^{(r)}/\partial \varepsilon$, small increments $\delta k_a^{(r)}$ and $\delta\varepsilon^{(r)}$ are given for $k_a^{(r)}$ and $\varepsilon^{(r)}$, respectively. After obtaining $\mathbf{T}_{\text{M}(k_a)}^{(r)} = f(k_a^{(r)} + \delta k_a^{(r)}, \varepsilon^{(r)}, \mathbf{T}^{(r)})$, and $\mathbf{T}_{\text{M}(\varepsilon)}^{(r)} = f(k_a^{(r)}, \varepsilon^{(r)} + \delta\varepsilon^{(r)}, \mathbf{T}^{(r)})$, we have

$$\begin{aligned} \frac{\partial \mathbf{T}_{\text{M}}^{(r)}}{\partial k_a} &\approx (\mathbf{T}_{\text{M}(k_a)}^{(r)} - \mathbf{T}_{\text{M}}^{(r)})/\delta k_a^{(r)}, \\ \frac{\partial \mathbf{T}_{\text{M}}^{(r)}}{\partial \varepsilon} &\approx (\mathbf{T}_{\text{M}(\varepsilon)}^{(r)} - \mathbf{T}_{\text{M}}^{(r)})/\delta\varepsilon^{(r)}. \end{aligned} \tag{14}$$

Then,

$$k_a^{(r+1)} = k_a^{(r)} + \Delta k_a^{(r)}, \quad \varepsilon^{(r+1)} = \varepsilon^{(r)} + \Delta\varepsilon^{(r)}. \tag{15}$$

2.4. Iterative steps and error assessment of reconstruction

The iterative calculation begins ($r = 0, 1, 2, \ldots$) from initial values $k_a^{(0)}$ and $\varepsilon^{(0)}$. (i) The temperature distribution $\mathbf{T}^{(r)}$ can be calculated from Eqs. (6)–(11). (ii) The updated radiative properties $k_a^{(r+1)}$ and $\varepsilon^{(r+1)}$ can be obtained from Eqs. (12)–(15). (iii) Return to (i) if the iterative number is not enough.

It can be seen that after the radiative properties approach the original ones, they begin to oscillate, but the oscillating magnitudes are not big. So, the iterative number can be determined after several trial calculations. Due to the oscillating of the radiative properties, their reconstruction results are the average values of the last five times. The reconstruction result for the temperature distribution is calculated from the averaged radiative properties. A reconstruction error for the temperature distribution is obtained as follows:

$$R_{\text{T}} = \left(\frac{1}{n} \sum_{i=1}^{n} (T_{\text{recons},i} - T_i)^2 \right)^{1/2} \Big/ \max(T_i). \tag{16}$$

Because we will study a sharp temperature distribution, the reconstruction error can also be assessed from the standard square deviations of the high temperatures and their relative errors. The reconstruction errors for the two radiative properties are also assessed from their standard square deviations and their relative errors.

3. Reconstruction results and discussion

The furnace system studied here [6,11] with dimension of 10 m × 10 m is shown in Fig. 2. The spatial re-

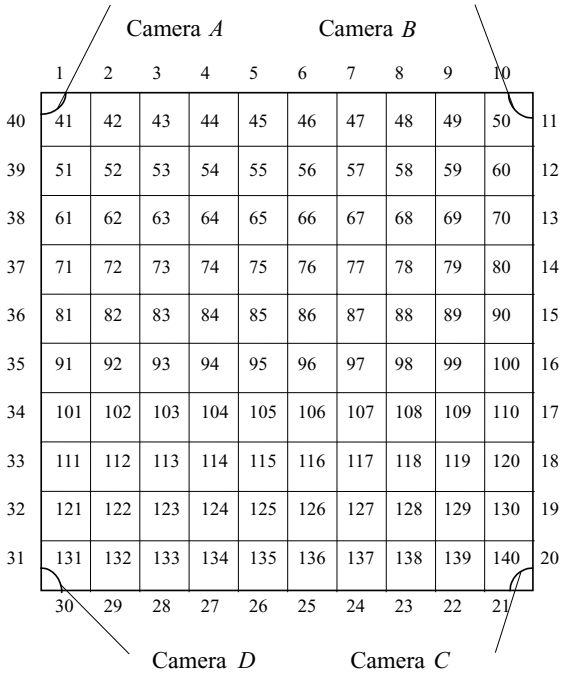

Fig. 2. The system studied with dimension of 10 m × 10 m. Sizing grid is 1 m × 1 m. Grid 1–40 refers to wall surface elements; others refer to gas elements [6].

gion is divided into $10 \times 10 = 100$ elements, and is surrounded by gray walls with an emissivity of 0.8. The absorption coefficient of the medium is assumed to be 0.1 m^{-1}. The wall is divided into $10 \times 4 = 40$ elements. Two cases are studied:

Case I. Wall surface temperature is 300 K, and a sharp temperature distribution in the medium is shown in Fig. 3(a);

Case II. The surface temperature is 800 K, and the temperature distribution shown in Fig. 3(b) is more smoother than that in Case I.

Four CCD cameras are mounted in the four corners with diameter of the lens assumed to be 0.47 m, which is larger than that for a real CCD camera. This choice is only for convenience of reducing calculation time [6,12]. The total angular field of view of the camera is assumed to be 100°, which is divided into 140 parts for the 140 image pixels of the CCD target. A two-color pyrometer is installed along the direction of the 70th image-formation element, which is close to the center line of the viewing field of the each camera.

The 1-D profiles/images of radiative energy **E**, temperatures $\mathbf{T}_C$ and $\mathbf{T}_M$ detected from the four corners in Case I are shown in Fig. 4(a)–(c), respectively. The peaks in the radiative energy profiles shown in Fig. 4(a) correspond to the three peaks of temperature in the system. All the four profiles of temperature $\mathbf{T}_C$ in Fig. 4(b) are almost straight lines within 1488 ± 2 K which nearly equal to the three high temperatures in the system, and the radiative energy emitted by these three high temperature elements would be much higher also. Due to the reflection of the wall surfaces, the monochromatic radiative energy emitted from these three high temperature elements dominates the energy received by all the image pixels. So, the temperatures calculated by Eq. (3) approach the high temperatures thereby.

The reference temperatures used for calculation of $\mathbf{T}_M$ are derived through the two-color method in Eq. (3), and then, they are all close to 1488 K as explained above. For the monochromatic radiative energy detected from corners A and C similar to that shown in Fig. 4(a), the peaks of radiative energy are higher than those at which the reference temperatures are measured. The temperature level of 2600 K in Fig. 4(c) deduced from

(a)

564.53	592.85	634.81	666.00	700.27	720.89	680.56	636.13	600.50	567.61
581.60	619.03	676.57	727.53	757.19	1489.51	735.71	667.78	623.79	589.37
589.05	630.52	709.98	1488.55	769.34	769.21	754.32	691.86	636.83	601.64
585.24	625.30	676.46	721.60	723.83	746.56	1487.92	709.45	637.17	596.68
578.06	605.76	637.18	657.01	676.41	701.62	723.06	671.14	623.25	584.63
564.41	580.81	604.40	622.19	635.55	642.30	646.30	626.66	602.60	571.52
546.95	558.91	581.36	597.31	597.32	599.94	607.10	592.84	575.93	552.43
526.66	543.60	559.23	567.55	573.36	577.39	570.16	562.05	554.80	532.69
508.10	523.56	534.12	542.87	552.51	550.08	548.57	545.85	530.12	513.22
493.80	499.17	520.10	519.65	526.85	530.69	529.72	520.92	504.54	490.77

(b)

800.00	800.00	800.00	800.00	800.00	800.00	800.00	800.00	800.00	800.00
800.00	917.19	1021.99	1064.86	1048.42	992.66	921.95	857.70	814.68	800.00
800.00	1088.81	1347.09	1452.75	1412.23	1274.82	1100.55	942.19	836.19	800.00
800.00	1210.30	1577.25	1727.36	1669.79	1474.57	1226.99	1002.01	851.41	800.00
800.00	1238.59	1630.82	1791.29	1729.75	1521.07	1256.43	1015.94	854.96	800.00
800.00	1176.41	1513.03	1650.75	1597.93	1418.84	1191.72	985.32	847.17	800.00
800.00	1057.65	1288.07	1382.34	1346.19	1223.60	1068.13	926.85	832.29	800.00
800.00	929.24	1044.83	1092.11	1073.98	1012.49	934.50	863.63	816.19	800.00
800.00	834.26	864.89	877.42	872.62	856.32	835.65	816.87	804.29	800.00
800.00	800.00	800.00	8 0000	800.00	800.00	800.00	800.00	800.00	800.00

Fig. 3. Two cases of temperature distributions, one in Case I (a) is sharper than the other in Case II (b).

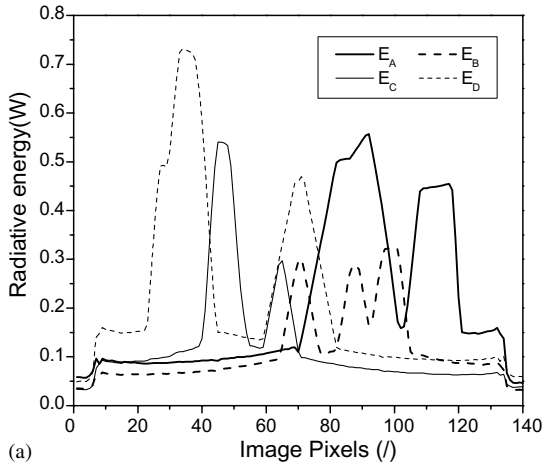

(a)

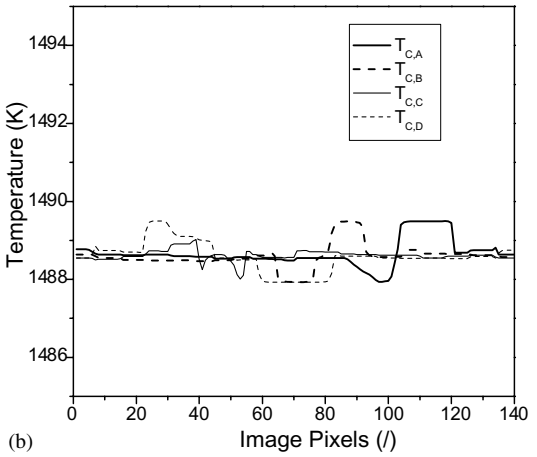

(b)

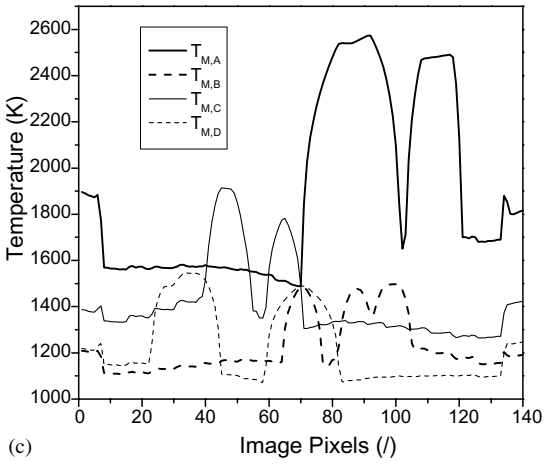

(c)

Fig. 4. The radiative energy profiles **E** (a) and the temperature profiles $\mathbf{T}_C$ (b) and $\mathbf{T}_M$ (c) in Case I.

Eq. (4) would be unreasonable. Contrarily, profiles of $\mathbf{T}_M$ obtained from corners B and D are more reasonable, since their reference temperatures are measured from the directions of peaks of radiative energy profiles. So, even if the radiative characteristics of the medium inside the system is gray, since the source of the radiative energy received from the boundary of the system is complicated, the radiative energy received from the system boundary is far from the spectroscopic features of a gray body, and the temperatures calculated from Wein's law maybe unacceptable.

Fig. 5 gives the iterative processes with standard deviation σ_s taking as 0.01, for the radiative properties when their initial values $k_a^{(0)}$ and $\varepsilon^{(0)}$ are guessed as $(0.2, 0.5)$, $(0.01, 0.5)$, $(0.01, 0.95)$, and $(0.2, 0.95)$ in Case I. It is obvious that even if the iterative processes are not the same for the different initial values and different random variables in Eq. (5), they all can converge to the vicinity of the original values with oscillations. One reason for the oscillations is that the calculation for the READ values of the image pixels with the Monte Carlo method has its own statistical errors [12]. But also, it maybe due to the individual updating of the temperature

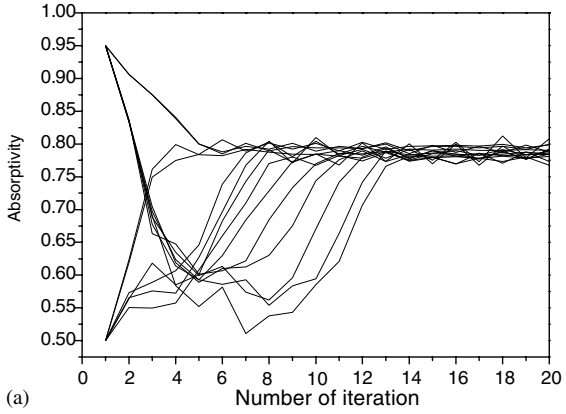

(a)

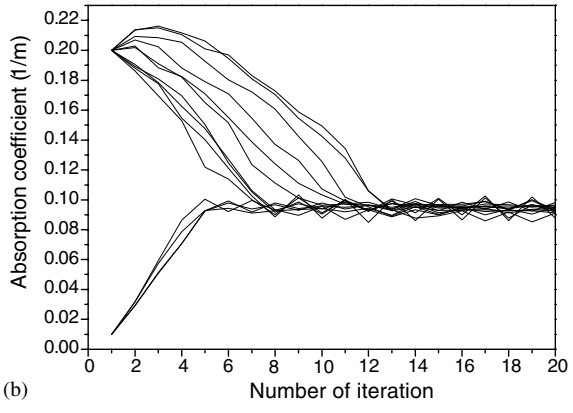

(b)

Fig. 5. The iterative processes (different calculation times with different random variables) (a) for k_a and (b) for ε with different initial values when $\sigma_s = 0.01$ in Case I.

	255.27	200.00	200.00	200.00	354.49	387.91	200.00	200.00	201.79	246.71	
240.09	586.45	712.01	599.88	200.00	781.26	733.81	663.36	642.70	627.14	603.14	248.06
295.87	536.55	658.31	743.80	306.20	842.16	1501.32	738.26	641.46	673.57	620.19	202.20
200.00	720.91	701.73	778.35	1441.98	912.50	853.31	696.06	780.69	657.84	625.16	200.00
389.62	711.06	710.96	862.76	200.00	932.51	823.44	1451.51	419.36	367.52	333.93	292.45
200.00	200.00	200.00	679.58	200.00	845.48	845.27	731.07	776.01	710.49	648.97	200.00
200.00	369.63	502.31	742.66	200.00	881.46	789.90	581.58	768.33	737.08	667.54	318.03
294.06	689.68	656.58	713.41	200.00	780.65	672.93	200.00	200.00	200.00	334.03	378.11
200.00	411.82	608.56	543.13	200.00	604.46	752.64	506.98	585.04	549.94	504.32	277.69
200.00	604.30	370.17	595.82	200.00	634.73	598.56	532.85	530.71	555.94	537.46	310.30
283.55	486.34	621.21	242.52	230.80	558.42	580.78	497.46	524.96	545.85	500.84	286.85
	267.33	200.00	301.40	322.78	321.01	296.18	330.23	200.00	228.11	275.82	

Fig. 6. One example of reconstructed temperature distributions in Case I. Inside the inner loop is for the medium and the outside is for the surface.

Table 1
Statistical results of the iteration calculations with $\sigma = 0.01$ in 14 times for Case I

	T_{56} (K)	T_{64} (K)	T_{77} (K)	k_a (1/m)	ε (/)	R_T
Original values	1489.51	1488.55	1487.93	0.10	0.80	/
Averaged values reconstructed	1496.89	1462.08	1461.43	0.09366	0.7878	9.03%
Standard square deviations of reconstructed values	8.637	28.05	27.91	0.006871	0.01390	1.28%
Relative errors of the reconstructed values	0.50%	1.78%	1.78%	6.34%	1.53%	/

distribution and the radiative properties. Fig. 6 displays one example of the results for the reconstruction of the temperature distributions. Statistical results for the values of radiative properties k_a and ε, and the three high temperatures T_{56}, T_{64}, T_{77} from 14 times of reconstruction with different random variables in Eq. (5) are summarized in Table 1. Because of the influence of the measurement errors, the reconstruction for the low temperature zone is not as good as that for the high temperature zone. The reconstruction errors R_T is 9.03% with a standard square deviation of 1.28%, which shows a good repeatability. In particular, the two radiative properties and the positions and the values of the three high temperature elements have been recovered very well, that is just interested for practical engineering.

Fig. 7 displays the iterative processes for Case II in 12 times of calculations with radiative properties k_a and ε when $\sigma_s = 0.01$ and different random variables of

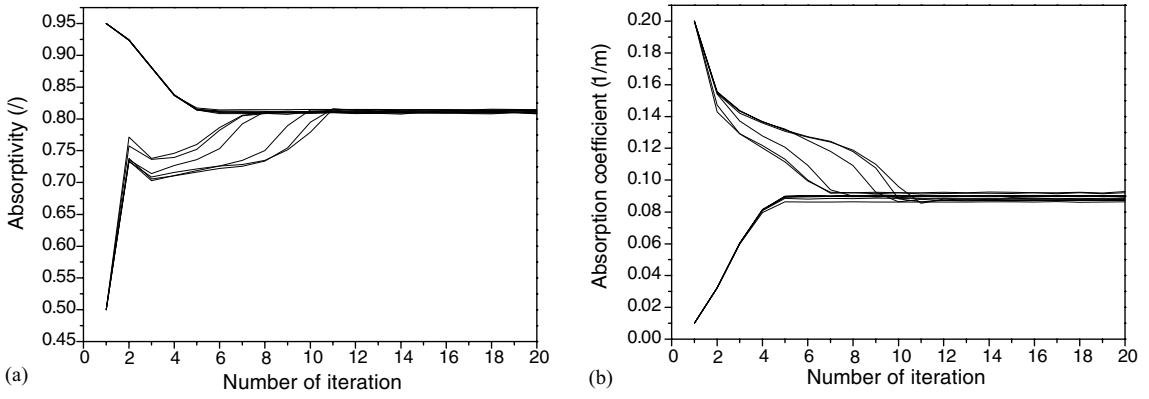

Fig. 7. The iterative processes in 12 times with $\sigma_s = 0.01$ and different initial values of (a) k_a and (b) ε for Case II.

Table 2
Statistical results for the iteration calculations with $\sigma = 0.01$ in 12 times for Case II

	T_{84} (K)	k_a (1/m)	ε (/)	R_T
Original values	1791.29	0.10	0.80	/
Averaged values reconstructed	1766.84	0.08925	0.8116	2.42%
Standard square deviations of reconstructed values	24.50	0.01090	0.01174	0.30%
Relative errors of the reconstructed values	1.36%	10.75%	1.45%	/

k_a and ε. Compared with those in Case I, the oscillating magnitudes of the radiative properties in Case II decrease obviously since the temperature distribution becomes smoother. It is seen, from summary of the reconstruction results listed in Table 2, the relative errors of the average values of the radiative properties are 10.75% and 1.45% for k_a and ε, respectively. They are similar to the levels obtained in Case I. However, the reconstruction results for the temperature distribution are more interesting, the reconstruction error R_T is 2.42%, which is much lower than that in Case I, where the relative error for the highest temperature, T_{84}, is 1.36% only. Fortunately, due to the strong mixing and heat transfer in industrial furnaces, the temperature distributions in them are smooth in general, which ensures the applicability of the simultaneous reconstruction method established in this paper.

4. Conclusions

A new method is proposed for the simultaneous estimation of absorption coefficient of the medium and absorptivity of the wall surface and temperature distributions in a two-dimensional furnace system. In this method, a revised Tikhonov regularization [10] is used to reconstruct temperature distribution from the radiative energy images, and the radiative properties are updated from the radiative temperature images, the radiative temperature images can serve as an additional measurement data besides the radiative energy images used in literatures [1–4].

For two cases, one with a sharper temperature distribution and the other with a smoother temperature distribution, respectively, taking account with normal distribution of standard square deviation of $\sigma = 0.01$ was added into the measurement data, the radiative properties can be reconstructed with errors from 1.45% to 10.75%. The positions and the values of the highest temperatures in the two cases were reconstructed well, which is more attractive in practice.

Acknowledgements

The present study has been supported by the Key Research Program of Ministry of Education of PR China (No. 99081), and the Teaching and Research Award Program for Outstanding Young Teachers in Higher Institutions of Ministry of Education of PR China. Part of this work was completed while the first author was staying at the Department of Mechanical and Nuclear Engineering, The Pennsylvania State University, USA, and the kindness and help of Professor M.F. Modest is acknowledged.

References

[1] M.P. Menguc, S. Manickavasagam, Inverse radiation problem in axisymmetric cylindrical scattering media, in: Fundamentals of Radiation Heat Transfer, HTD, vol. 160, ASME, 1991, pp. 61–68.
[2] H.Y. Li, Inverse radiation problem in two-dimensional rectangular media, J. Thermophys. Heat Transfer 11 (1997) 556–561.
[3] A.J.S. Neto, M.N. Özisik, An inverse problem of simultaneous estimation of radiation phase function, albedo and optical thickness, J. Quant. Spectrosc. Radiat. Transfer 53 (1995) 397–409.
[4] H. Erturk, A. Ezekoye, J.R. Howell, Inverse solution of radiative transfer in two-dimensional irregularly shaped enclosures, in: HTD, vol. 366-1, ASME, 2000, pp. 109–117.
[5] H.C. Zhou, P. Yuan, F. Sheng, C.G. Zheng, Simultaneous estimation of the profiles of the temperature and the scattering albedo in an absorbing, emitting and isotropically scattering medium by inverse analysis, Int. J. Heat Mass Transfer 43 (2000) 4361–4364.
[6] H.C. Zhou, F. Sheng, S.D. Han, Y.L. Huang, C.G. Zheng, Reconstruction of temperature distribution in a 2-D absorbing–emitting system from radiant energy images, JSME Int. J., Ser. B 43 (2000) 104–109.
[7] A.N. Tikhonov, Solution of incorrectly formulated problems and the regularization method, Soviet Math. Dokl. 4 (1963) 1035–1038.
[8] A. Neumaier, Solving ill-conditioned and singular linear systems: a tutorial on regularization, SIAM Rev. 40 (1998) 636–666.
[9] T. Reginska, A regularization parameter in discrete ill-posed problems, SIAM J. Sci. Comput. 17 (1996) 740–749.
[10] J.P. Holloway, S. Shannon, S.M. Sepke, M.L. Brake, A reconstruction algorithm for a spatially resolved plasma optical emission spectroscopy sensor, J. Quant. Spectrosc. Radiat. Transfer 68 (2001) 101–115.
[11] K. Kudo, A. Kuroda, T. Saito, Solution of the inverse radiative load problem using the singular value decompo-

sition technique, JSME Int. J., Ser. B 39 (1996) 808–814.

[12] H.C. Zhou, F. Sheng, S.D. Han, C.G. Zheng, A fast algorithm for calculation of radiative energy distributions received by pinhole image-formation process from 2-D rectangular enclosures, Numer. Heat Transfer, Part A: Appl. 38 (2000) 757–773.

[13] H.C. Zhou, S.S. Zhang, Y.L. Huang, C.G. Zheng, Monitoring of 2-D combustion temperature images in a 670t/h utility boiler and simulation on its application in combustion control, Dev. Chem. Eng. Mineral Process 8 (2000) 311–322.

[14] B.C. Young, D.P. McCollor, B.J. Weber, M.L. Jones, Temperature measurements of Beulah lignite char in a novel laminar flow reactor, Fuel 67 (1988) 40–44.

[15] H.C. Zhou, S.D. Han, F. Sheng, C.G. Zheng, Visualization of three-dimensional temperature distributions in a large-scale furnace via regularized reconstruction from radiative energy images: numerical studies, J. Quant. Spectrosc. Radiat. Transfer 72 (2002) 361–383.